
High-resolution spectroscopy of the extremely iron-poor post-AGB star CC Lyr

Wako AOKI^{1,2}, Tadafumi MATSUNO², Satoshi HONDA³, Mudumba PARTHASARATHY⁴, Haining LI⁵ and Takuma SUDA⁶

¹National Astronomical Observatory, 2-21-1 Osawa, Mitaka, Tokyo 181-8588, Japan

²Department of Astronomical Science, School of Physical Sciences, The Graduate University of Advanced Studies (SOKENDAI), 2-21-1 Osawa, Mitaka, Tokyo 181-8588, Japan

³Center for Astronomy, University of Hyogo, 407-2, Nishigaichi, Sayo-cho, Sayo, Hyogo 679-5313, Japan

⁴Indian Institute of Astrophysics, II Block, Koramangala, Bangalore 560 034, INDIA

⁵Key Lab of Optical Astronomy, National Astronomical Observatories, Chinese Academy of Sciences, A20 Datun Road, Chaoyang, Beijing 100012, China

⁶Research Center for the Early Universe, University of Tokyo, 7-3-1 Hongo, Bunkyo-ku, Tokyo 113-0033, Japan

*E-mail: aoki.wako@nao.ac.jp, tadafumi.matsuno@nao.ac.jp, honda@nhao.jp, m-partha@hotmail.com, lhn@nao.cas.cn, suda@resceu.s.u-tokyo.ac.jp

Received (reception date); Accepted (acceptation date)

Abstract

High-resolution optical spectroscopy was conducted for the metal-poor post-AGB star CC Lyr to determine its chemical abundances and spectral line profiles. Our standard abundance analysis confirms its extremely low metallicity ($[\text{Fe}/\text{H}] < -3.5$) and a clear correlation between abundance ratios and the condensation temperature for 11 elements, indicating that dust depletion is the cause of the abundance anomaly of this object. The very low abundances of Sr and Ba, which are detected for the first time for this object, suggest that heavy neutron-capture elements are not significantly enhanced in this object by the s-process during its evolution through AGB phase. Radial velocity of this object and profiles of some atomic absorption lines show variations depending on pulsation phases, which could be formed by dynamics of the

atmosphere rather than by binarity or contributions of circumstellar absorption. On the other hand, the $H\alpha$ emission with double peaks shows no evident velocity shift, suggesting that the emission is originating from the circumstellar matter, presumably the rotating disk around the object.

Key words: stars:abundances — stars:AGB and post-AGB — circumstellar matter — stars:individual (CC Lyr)

1 Introduction

A small number of warm post-AGB stars are known to show anomalously low abundances of Fe and other metals. BD+39°4926, HR 4049, HD 44179 and HD 52961 are known to have $[Fe/H] < -3$ (Waelkens et al. 1991; Van Winckel et al. 1995). Most metals including Fe are highly depleted in these stars, whereas some volatile elements, e.g., C, O, S, Zn, are not depleted as significant as Fe, indicating that formation and ejection of dust from these objects are the cause of depletion of refractory elements.

Although no convincing models have yet been established, scenarios to explain this phenomenon have been proposed. The basic idea is that, after a circumstellar shell is formed by efficient mass-loss during the evolution along the asymptotic giant branch, the gas component is re-accreted onto the surface of the star. The dust component that contains most metals of the ejected material is removed in the process (Mathis & Lamers 1992). This specific process may operate in circumstellar disk that is formed in a binary system with a low-mass companion star (Waters et al. 1992). Indeed, binarity is confirmed for the four extremely metal-poor post-AGB stars mentioned above (Van Winckel et al. 1995).

CC Lyr is a high galactic latitude star ($b = 17.23^\circ$) and is classified as a Type II Cepheid based on its light curve (e.g., Schmidt et al. 2004). The abundance analysis for this object by Maas et al. (2007), however, revealed that refractory elements show large depletion (e.g., $[Fe/H] = -3.5$), as found for some post-AGB stars as mentioned above, indicating that this object is an extremely metal-poor post-AGB star.

Other features of this object also support the interpretation that this object is a post-AGB star. One is the pulsation and its period (24.23 days), which is similar to the periods previously found for other metal-poor post-AGB stars. A significant excess of infrared emission is also found, as the case of other post-AGB stars. We note that the class of Type II Cepheids consists of many types of

objects, including post-AGB stars like RV Tau stars (Wallerstein 2002).

This object was re-discovered as a candidate of extremely metal-poor star by the spectroscopic survey with the Large sky Area Multi-Object fiber Spectroscopic Telescope (LAMOST; Cui et al. 2012). High-resolution spectra of this object were obtained with the Subaru Telescope during a follow-up program. We here report our new measurement of chemical abundances, radial velocities and absorption line profiles of this object.

2 Observations

The object was identified to be a candidate of a metal-poor star by the medium resolution ($R \sim 1800$) spectroscopy with LAMOST in its regular survey (Zhao et al. 2012). The ID in the LAMOST survey is LAMOST J 1833+3138. Figure 1 shows the LAMOST spectrum of this object. The spectral features are very similar to those of carbon-enhanced metal-poor (CEMP) stars, except for the emission feature of $H\alpha$.

High resolution ($R = 45,000$) spectra of this object were obtained with the Subaru Telescope High Dispersion Spectrograph (HDS; Noguchi et al. 2002) in a program (S16A-119I) for follow-up spectroscopy for metal-poor star candidates found with LAMOST (Li et al. 2015). Since the object is bright ($V \sim 12$), observations were conducted using the twilight time in the Subaru program.

Observations with the Subaru/HDS were made at three epochs in April and May 2016 (Table 1). The pulsation phase is calculated using the light curve parameters obtained by Schmidt et al. (2004). Recent photometry data provided by AAVSO ¹ suggest that the phase possibly has offset by at most 0.1, but confirm that our observations were made in the late half of the phase, and the first two were done at almost the same phase.

Standard data reduction procedures were carried out with the IRAF echelle package². The wavelength shift due to earth's orbital motion is corrected using the IRAF task *rvcor*.

3 Chemical composition

3.1 Measurements of spectral lines

The absorption lines measured from the spectra are given in Table 2. Many C I lines are detected in the spectra, as expected from the previous studies. Line data of most of the C I lines are taken from Takeda et al. (2002) who have studied the spectrum of the metal-poor post-AGB star HR 4049. Line

¹ <https://www.aavso.org>

² IRAF is distributed by the National Optical Astronomy Observatories, which is operated by the Association of Universities for Research in Astronomy, Inc. under cooperative agreement with the National Science Foundation.

data for other spectral features are taken from studies on very metal-poor stars (e.g., Aoki et al. 2013).

Strong absorption features have asymmetry as shown in Figure 2. The asymmetry is in particular evident in the first two spectra obtained at $\phi \sim 0.7$, whereas the lines are almost symmetrical in the other spectrum. The variation of the line profiles is discussed in § 4.

We measure equivalent widths (W) by fitting a Gaussian profile. Since strong lines in the spectrum of April 27 show asymmetry as depicted in Figure 2, we measure the equivalent widths by direct integration for lines with $\log W/\lambda > -5.0$ in the spectrum. The measured equivalent widths are given in Table 2 with line data used in the abundance analysis.

3.2 Stellar parameters and abundance analysis

Model atmospheres of the ATLAS NEWODF grid (Castelli et al. 1997) are applied to our 1D/LTE analysis.

We started the analysis of the spectrum obtained on 27 April adopting the stellar parameters given by Maas et al. (2007): $T_{\text{eff}} = 6250$ K, $\log g = 1.0$ and $v_{\text{turb}}=3.5$ km s⁻¹. We found that the Fe abundances derived from the Fe I lines is about 0.5 dex higher than that from the Fe II ones for this parameter set. This discrepancy is reduced by assuming higher gravity and lower effective temperature. Hence, we adopt $T_{\text{eff}} = 6000$ K and $\log g = 2.0$. Abundance results are given in Table 3.

As found by Maas et al. (2007), this object has CNO abundances as high as that of the Sun, but very low abundances of most of other metals including Fe. Hence, its chemical composition is not approximated by the scaled-solar metal abundances. We examined model atmospheres for two extreme cases of metallicity, $[M/H] = -0.5$ and -3.5 . The difference of elemental abundances obtained by the two models is less than 0.2 dex, and less than 0.1 dex in most cases (Table 4), which does not affect the following discussions. We adopt the model of $[X/H] = -0.5$ to obtain the final result.

The microturbulent velocity is uncertain due to the limited number of spectral lines used for deriving abundances for each element. We modified the value as the derived carbon abundances from individual C I lines is independent of the strengths of the lines used in the analysis. The adopted value is $v_{\text{turb}}=4.5$ km s⁻¹, which is larger than that of Maas et al. (2007). The effect of the changes of v_{turb} on the derived abundances is, however, almost negligible (Table 4).

The carbon abundance is determined by the measurements of 13 C I lines. The abundance is also estimated by the comparison of synthetic spectra for CH molecular band at 4322 Å with observed ones (Figure 3). The carbon abundance assumed for the calculation for the spectrum obtained on April 27 is $[C/H] = -0.33$, which agrees with the result from C I lines within the measurement error.

The CH band is sensitive to the effective temperature adopted by the analysis. The agreement of the abundances from C I lines and the CH band supports the effective temperature adopted in the analysis.

The abundances of other elements are derived by the standard analysis for the measured equivalent widths.

The spectrum obtained on May 21 is almost identical to that of April 27, and the S/N ratio is not as good as the first one. We do not conduct abundance analysis for the May 21st spectrum. On the other hand, the spectrum of May 29 shows significant changes of absorption features from the other two spectra. As found in Figure 3, the CH band is stronger in this spectrum, indicating that the temperature is lower at this epoch. We assume $T_{\text{eff}} = 5750$ K for the analysis of the May 29 spectrum.

The equivalent widths measured for lines with high excitation potential in the May 29 spectrum are smaller than those in the April 27th one, whereas the trend is opposite for lines with low excitation potential (Table 4). This supports the lower T_{eff} on May 29. Thanks to the lower temperature, the two Ba II lines are detected in the spectrum of May 29. The two Sr II resonance lines are clearly detected in both spectra. The abundances of heavy neutron-capture elements are measured for the first time for CC Lyr. The effect of hyperfine splitting is ignored because the spectral lines analyzed in the present work are sufficiently weak.

3.3 Abundance ratios and correlation with condensation temperature

The elemental abundances derived by our analysis are plotted as a function of the condensation temperature in Figure 4. As found by Maas et al. (2007), a clear correlation between the abundances and the condensation temperature is found. This correlation confirms that the refractory elements with high condensation temperature are severely depleted by condensation to dust grains that are removed from the material preserved at the surface of the star.

The S and Zn abundances are slightly lower than the solar value, and the ratio [Zn/S] is about -0.5 . These values are along the trend found by previous studies for metal-poor post-AGB stars including CC Lyr (Takeda et al. 2002; Maas et al. 2007). If the abundances of these two elements with low condensation temperature primarily trace the initial metallicity of this object, it should be a slightly metal-poor, and would be a low-mass object with a long life-time. This is consistent with the masses of metal-poor post-AGB stars estimated by Bono et al. (1997) and Gingold (1985) to be in the range of 0.52 to $0.59 M_{\odot}$.

Our measurements provide new data points of heavy neutron-capture elements, Sr and Ba, which could be produced by the s-process during the evolution along the asymptotic giant branch. There is no excess of these elements in this object compared to the trend in Figure 4: if the correlation

between the condensation temperature and elemental abundances found for most metals are extended to those of Sr and Ba, which have the highest condensation temperature, additional s-process contribution to this object should be small if any. The typical mass of AGB stars in which s-process is active is estimated to be $1.5\text{--}3 M_{\odot}$ (Käppeler et al. 2011). The minimum core mass to trigger the third dredge-up predicted by stellar evolutionary models ranges between $0.5\text{--}0.6 M_{\odot}$ (Stancliffe et al. 2005; Weiss & Ferguson 2009; Cristallo et al. 2011) or higher (Iben 1981). This is also consistent with the mass estimates for metal-poor post-AGB stars mentioned above.

4 Dynamics

In the high resolution spectra of CC Lyr obtained by the present work, variations and asymmetry of absorption features are found. $H\alpha$ is observed as emission with double peaks. This section reports these spectral features for the spectra obtained at the three epochs. We note that no clear circumstellar absorption of C_2 molecule is detected for CC Lyr, in contrast to another very metal-poor AGB star HD 52961 (Bakker et al. 1996). Na I D lines show complicated absorption features, in addition to the photospheric absorption. The absorption features, however, appear at longer wavelengths than the photospheric ones, which is not simply explained by circumstellar absorption formed in an expanding shell. These absorption features would be primarily due to interstellar absorption, as found in the Na I of HR 4049 (Bakker et al. 1998).

4.1 Radial velocities

The radial velocity of the object is measured by the wavelength shift of the core of the six absorption lines of Mg, Fe and Zn. The derived values are given in Table 1. The error given in the table is standard deviation of the measurements. Including possible systematic errors due to instability of the spectrograph, the uncertainty of the measurement could be as large as 0.5 km s^{-1} .

The three epochs of the observations correspond to the phase of the light curve (ϕ) of 0.7, 0.7 and 1.0 for April 27, May 21, and May 29, respectively. The radial velocities measured for the first two observations at $\phi = 0.7$ are almost identical, whereas the other at $\phi = 1.0$ is 11 km s^{-1} larger. This suggests that the radial velocity change is related to the pulsation of the object, although definitive conclusion cannot be derived from the three measurements.

Taking the binarity found for other metal-poor post-AGB stars into consideration, this object is expected to belong to a binary system with an orbital period of several hundred days (Van Winckel et al. 1995). In order to examine the binarity of this object from radial velocity changes, long-range monitoring that can distinguish the effect of the pulsation and orbital motion in the binary system is

required.

4.2 Asymmetry of absorption profiles

Strong C I lines show asymmetry in the spectra obtained on April 27 and May 21. Figure 2 shows the line profiles in a velocity scale. The profile is empirically reproduced by assuming two components of Gaussian with 15 km s^{-1} separation. Similar asymmetry of absorption line profile is found for HD 52961. Kipper (2013) analyzed the profile assuming two Gaussian components and discussed the weaker blue component as absorption by expanding circumstellar shell.

The asymmetry is, however, not evident in the spectrum of CC Lyr obtained on May 29 at a different pulsation phase (Figure 2). There is no detectable absorption at the velocity of $\sim -50 \text{ km s}^{-1}$ at which a “blue component” is found in the other two spectra. This indicates that the blue component is also formed in the dynamic photosphere, or the expanding circumstellar shell appears only in a limited phases of the pulsation.

4.3 $H\alpha$ emission

Figure 5 shows the velocity profile of the $H\alpha$ emission in the spectra. By contrast to the C I absorption, $H\alpha$ emission shows no detectable velocity shift, although the profile and strength of the double peaks slightly change.

CC Lyr seems to be very similar to the very metal-poor post-AGB binary stars HD 52961 and IRAS 11472-0800 ($[\text{Fe}/\text{H}] = -2.7$; Van Winckel et al. 2012). The $H\alpha$ profile of IRAS 11472-0800 with double peaks and its variation reported by Van Winckel et al. (2012) seems to be very similar to those of CC Lyr.

Emission of $H\alpha$ is also observed in the very metal-poor post-AGB star HR 4049 (Bakker et al. 1998). The feature found for HR 4049 consists of strong emission of the red component, and the weak blue component shows significant variation, which seems to be more complicated than the emission feature of CC Lyr. Bakker et al. (1998) discuss two possible models to explain the $H\alpha$ emission of HR 4049: one is the circumbinary disk that reflects the light of the post-AGB star. The variation of the emission feature is explained by assuming that only a small portion of the disk reflects the light. If similar model is applied to the $H\alpha$ emission of CC Lyr, the clear double peak, without significant time variation, suggests that a larger part of the disk reflects the star light. The other model is the activity in the extended atmosphere like the chromosphere. In the case of CC Lyr, no correlation between $H\alpha$ and the pulsation period suggests this model is unlikely, though further monitoring of the emission feature is required to clearly distinguish the two models.

5 Discussion and concluding remarks

Our abundance measurements for CC Lyr based on high resolution spectroscopy confirmed the low abundances of metals with high condensation temperatures, that indicate significant effects of dust depletion on the surface composition of this object, as found in several post-AGB stars with extremely low metallicity (Van Winckel et al. 1995). Low abundances of Sr and Ba, which are detected for the first time for this object in the phase with low temperature suggests that s-process was not very effective during its AGB phase.

CC Lyr is a very metal-poor post-AGB supergiant similar to HD 52961 and IRAS 11472-0800, which have relatively low temperatures ($T_{\text{eff}} \sim 6000$ K) among several objects in this class. The radial velocity variations indicate that it may be a single lined spectroscopic binary similar to HD 52961 and other very metal-poor post-AGB stars. However, to disentangle the radial velocity variations due to pulsation and binarity needs very long period monitoring of the radial velocity variations.

Our high-resolution spectroscopy for CC Lyr also revealed the asymmetry of absorption features and their variation with pulsation phases. This is similar to that found in the very metal-poor post-AGB star HD 52961. Similar line profile asymmetry seems to be common in post-AGB stars, as they have very extended atmospheres and velocity fields due to mass motions etc. Plane parallel approximation and LTE conditions may not be very suitable to analyze the spectra of these stars. However, the agreements of abundance results for different pulsation phases support that the overall abundance features found in the present work, in particular the correlation with condensation temperatures of elements, are robust.

The emission feature of $H\alpha$ found in CC Lyr could be key to probing the structure of circumstellar disk. The double peak emission does not show clear correlation with the pulsation phase, although the number of observations is still limited. The feature is similar to those found in other post-AGB stars, in particular IRAS 11472-0800 (Van Winckel et al. 2012). Monitoring $H\alpha$ emission for CC Lyr and other metal-poor post-AGB stars, as done by Bakker et al. (1998) for HR 4049, will help us understand the circumstellar matter of post-AGB stars in general.

The group of post-AGB stars with very low metallicity still consists of a small number of objects including CC Lyr. Their features are, however, more or less found in many post-AGB stars. The pulsation period of CC Lyr (24.3 days) and amplitude of the light curve of CC Lyr indicates it is in the border region of W Vir type Type II Cepheids and RV Tau stars (Wallerstein 2002). $H\alpha$ emission profile is observed in the spectra of many W Vir type Type II Cepheids. Lemasle et al. (2015) find $H\alpha$ emission profile somewhat similar to that found in the spectrum of CC Lyr in a few Type II Cepheids of W Vir class. They also find mild depletion of refractory elements indicating dust gas separation.

Gonzalez & Wallerstein (1996) found that the Type II Cepheid ST Pup is a single lined spectroscopic binary with a dusty disk and depletion of Fe and other refractory elements similar to that of CC Lyr. In more general, interaction of circumstellar matter and a companion star in a binary system seems to play essential role in the evolution of post-AGB star and formation of planetary nebulae. Continuous study of metal-poor post-AGB stars like CC Lyr will contribute to the understanding of the late phase of low-mass star evolution.

Acknowledgments

This work is based on data collected at the Subaru Telescope, which is operated by the National Astronomical Observatory of Japan. WA and TS were supported by JSPS KAKENHI Grant Numbers JP16H02168. MP was supported by the NAOJ Visiting Fellow Program of the Research Coordination Committee, National Astronomical Observatory of Japan (NAOJ), National Institutes of Natural Sciences(NINS).

References

- Aoki, W., Beers, T. C., Lee, Y. S., et al. 2013, *AJ*, 145, 13
- Asplund, M., Grevesse, N., Sauval, A. J., & Scott, P. 2009, *ARA&A*, 47, 481
- Bakker, E. J., Waters, L. B. F. M., Lamers, H. J. G. L. M., Trams, N. R., & van der Wolf, F. L. A. 1996, *A&A*, 310, 893
- Bakker, E. J., Lambert, D. L., Van Winckel, H., et al. 1998, *A&A*, 336, 263
- Bono, G., Caputo, F., & Santolamazza, P. 1997, *A&A*, 317, 171
- Castelli, F., Gratton, R. G., & Kurucz, R. L. 1997, *A&A*, 318, 841
- Cristallo, S., Piersanti, L., Straniero, O., et al. 2011, *ApJS*, 197, 17
- Cui, X.-Q., Zhao, Y.-H., Chu, Y.-Q., et al. 2012, *Research in Astronomy and Astrophysics*, 12, 1197
- Gingold, R. A. 1985, *Mem. Soc. Astron. Italiana*, 56, 169
- Gonzalez, G., & Wallerstein, G. 1996, *MNRAS*, 280, 515
- Iben, I., Jr. 1981, *ApJ*, 246, 278
- Käppeler, F., Gallino, R., Bisterzo, S., & Aoki, W. 2011, *Reviews of Modern Physics*, 83, 157
- Kipper, T. 2013, *Baltic Astronomy*, 22, 101
- Lemasle, B., Kovtyukh, V., Bono, G., et al. 2015, *A&A*, 579, A47
- Li, H., Aoki, W., Zhao, G., et al. 2015, *PASJ*, 67, 84
- Maas, T., Giridhar, S., & Lambert, D. L. 2007, *ApJ*, 666, 378
- Mathis, J. S., & Lamers, H. J. G. L. M. 1992, *A&A*, 259, L39
- Noguchi, K., Aoki, W., Kawanomoto, S., et al. 2002, *PASJ*, 54, 855
- Schmidt, E. G., Johnston, D., Langan, S., & Lee, K. M. 2004, *AJ*, 128, 1748

- Stancliffe, R. J., Izzard, R. G., & Tout, C. A. 2005, MNRAS, 356, L1
- Takeda, Y., Parthasarathy, M., Aoki, W., et al. 2002, PASJ, 54, 765
- Van Winckel, H., Hrivnak, B. J., Gorlova, N., Gielen, C., & Lu, W. 2012, A&A, 542, A53
- Van Winckel, H., Waelkens, C., & Waters, L. B. F. M. 1995, A&A, 293,
- Waelkens, C., Van Winckel, H., Bogaert, E., & Trams, N. R. 1991, A&A, 251, 495
- Wallerstein, G. 2002, PASP, 114, 689
- Waters, L. B. F. M., Trams, N. R., & Waelkens, C. 1992, A&A, 262, L37
- Weiss, A., & Ferguson, J. W. 2009, A&A, 508, 1343
- Zhao, G., Zhao, Y.-H., Chu, Y.-Q., Jing, Y.-P., & Deng, L.-C. 2012, Research in Astronomy and Astrophysics, 12, 723

Table 1. Observations

Observation date (UT)	HJD	Phase	$V_{\text{Helio}}(\text{km s}^{-1})$
April 27, 2016	2457506.09	0.68	-36.5 ± 0.2
May 21, 2016	2457530.00	0.67	-36.1 ± 0.6
May 29, 2016	2457538.00	1.00 (0.00)	-25.1 ± 0.3

Table 2. Equivalent widths

Ion	Wavelength (Å)	$\log gf$	χ (eV)	W (mÅ)April 27	W (mÅ)May 29
C I	4766.67	-2.51	7.48	16.3
C I	4770.03	-2.33	7.48	30.7	26.3
C I	4771.74	-1.76	7.49	96.1	64.7
C I	4775.90	-2.19	7.49	48.3	33.7
C I	4817.37	-2.89	7.48	19.0	11.7
C I	4826.80	-3.05	7.49	9.8
C I	4932.05	-1.66	7.69	73.1	52.9
C I	5023.85	-2.21	7.95	13.5
C I	5024.92	-2.73	7.95	4.3
C I	5039.06	-1.79	7.95	36.7
C I	5040.13	-2.30	7.95	20.5
C I	5052.17	-1.30	7.69	129.4	79.5
C I	5793.12	-2.16	7.95	20.4
C I	6013.21	-1.47	8.65	13.7
C I	6014.83	-1.71	8.64	17.9
C I	6587.61	-1.60	8.54	48.1
O I	5577.34	-8.20	1.97	20.8	26.1
O I	6300.30	-9.82	0.00	72.6	78.0
O I	6363.78	-10.30	0.02	19.6	35.4
Na I	5682.63	-0.70	2.10	11.1	21.0
Na I	5688.00	-0.46	2.10	18.2
Mg I	5167.32	-0.86	2.71	22.0	42.8
Mg I	5172.68	-0.45	2.71	45.6	59.1
Mg I	5183.60	-0.24	2.72	68.6	72.0
S I	4694.11	-1.77	6.52	21.9	13.3
S I	4695.44	-1.92	6.52	11.3	9.5
S I	4696.25	-2.14	6.52	5.9
S I	6052.67	-0.74	7.87	18.4	16.8
S I	6757.17	-0.31	7.87	43.4	33.9
Mn I	4030.75	-0.50	0.00	23.0	50.7
Mn I	4033.06	-0.62	0.00	18.6	37.0

Table 2. (Continued)

Ion	Wavelength (\AA)	$\log gf$	$\chi(\text{eV})$	$W(\text{m\AA})$ April 27	$W(\text{m\AA})$ May 29
Fe I	4383.54	0.21	1.49	54.7	74.3
Fe I	4404.75	-0.15	1.56	30.0	47.1
Fe I	4415.12	-0.62	1.61	19.0	28.3
Fe I	4957.60	0.23	2.81	11.5
Zn I	4680.13	-0.81	4.01	17.9	32.0
Zn I	4722.15	-0.39	4.03	47.3	61.3
Zn I	4810.53	-0.17	4.08	60.2	78.2
Zn I	6362.34	0.15	5.80	14.8
Fe II	4923.93	-1.21	2.89	20.5	49.0
Fe II	5169.00	-0.87	2.89	40.6	21.6
Sr II	4077.71	0.16	0.00	45.7	62.9
Sr II	4215.52	-0.16	0.00	22.1	49.2
Ba II	4554.03	0.16	0.00	8.8
Ba II	4934.08	-0.15	0.00	7.1

Table 3. Chemical Composition of CC Lyr

			April 27 data			May 29 data		
T_{eff}			6000 K			5750 K		
$\log g$			2.0			2.0		
[X/H]			-0.5			-0.5		
v_{turb}			4.5 km s $^{-1}$			4.5 km s $^{-1}$		
Element	Ion	$\log \epsilon_{\odot}$	[X/H]	n	σ_{total}	[X/H]	n	σ_{total}
C	C I	8.43	-0.11	13	0.18	-0.23	9	0.20
O	O I	8.69	0.35	3	0.23	0.40	3	0.23
Na	Na I	6.24	-1.35	2	0.18	-1.13	1	0.18
Mg	Mg I	7.60	-3.64	3	0.22	-3.60	3	0.24
S	S I	7.12	-0.39	5	0.12	-0.42	4	0.15
Mn	Mn I	5.53	-3.54	2	0.33	-3.40	2	0.36
Fe	Fe I	7.50	-3.85	4	0.26	-3.90	3	0.31
Fe	Fe II	7.50	-4.04	2	0.21	-4.09	2	0.22
Zn	Zn I	4.56	-1.02	3	0.22	-0.89	4	0.21
Sr	Sr II	2.87	-4.35	2	0.26	-4.17	2	0.27
Ba	Ba II	2.18	-4.22	2	0.25

Table 4. Abundance sensitivity to stellar parameters

Element	δT_{eff}	$\delta \log g$	δv_{turb}	$\delta[\text{M}/\text{H}]$	r.s.s.
	+250 K	-0.5 dex	-0.5 km s ⁻¹	-3.0 dex	
C	-0.08	-0.14	0.02	0.07	0.17
O	0.11	-0.16	0.01	-0.05	0.20
Na	0.10	0.01	0.00	-0.08	0.13
Mg	0.15	0.00	0.01	-0.12	0.20
S	-0.02	-0.10	0.01	0.02	0.10
Mn	0.24	0.00	0.01	-0.19	0.30
Fe	0.19	0.00	0.01	-0.16	0.25
Fe	0.04	-0.17	0.01	-0.04	0.17
Zn	0.15	-0.01	0.01	-0.12	0.20
Sr	0.13	-0.17	0.01	-0.09	0.23
Ba	0.13	-0.18	0.00	-0.12	0.25

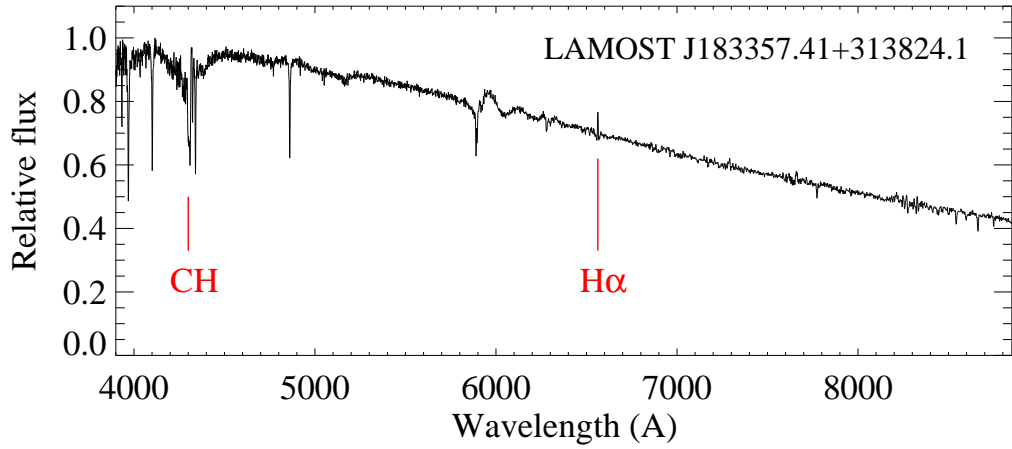


Fig. 1. The medium-resolution spectrum of CC Lyr (LAMOST J 183357.41+313824.1) obtained with LAMOST. The position of CH G-band and H α (emission) are presented.

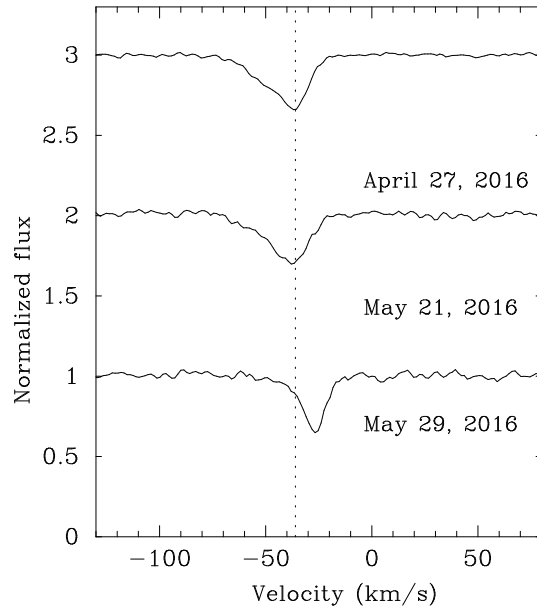


Fig. 2. The absorption feature of C I 5052 Å line. The spectra of April 27 and May 21 are vertically shifted. The vertical dotted line is the radial velocity determined from other absorption lines for the April 27 spectrum.

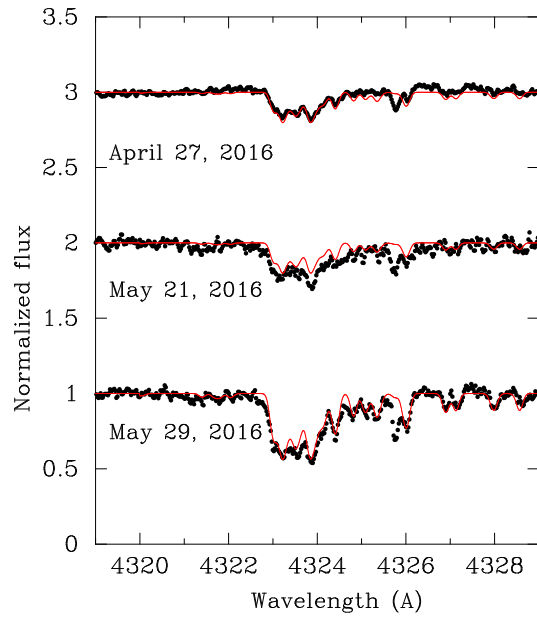


Fig. 3. The CH $A - X$ band of CC Lyr obtained at three epochs (dots). The spectra of April 27 and May 21 are vertically shifted. The red lines are synthetic spectra for $T_{\text{eff}} = 6000$ K for the spectra obtained on April 27 and May 21 and for $T_{\text{eff}} = 5750$ K for the May 29 spectrum.

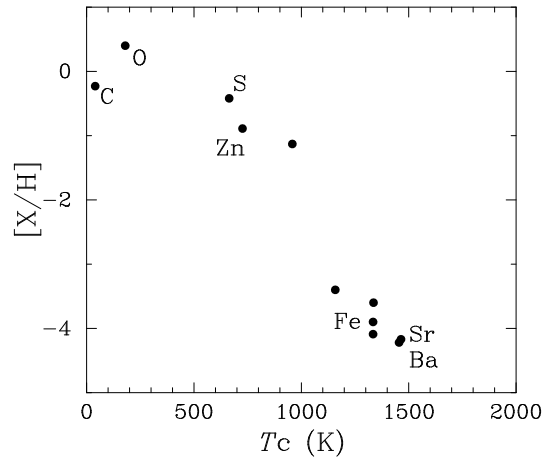


Fig. 4. Derived elemental abundance ratios ($[X/H]$) as a function of the condensation temperatures.

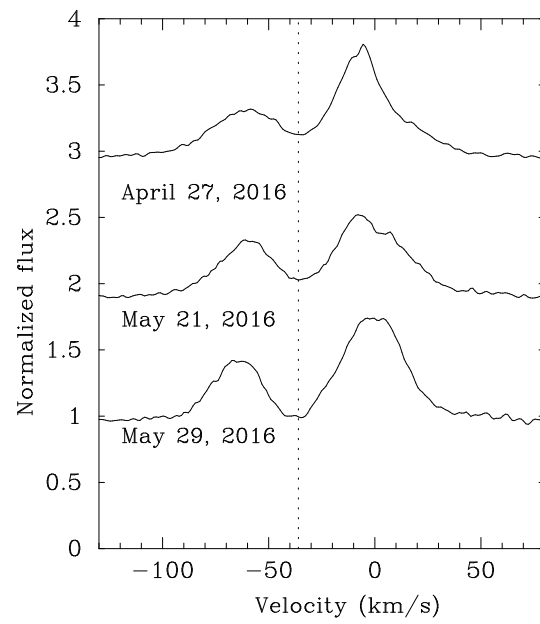


Fig. 5. The same as Figure 2, but for the emission feature of H α .